Prediction of response for vortex-induced vibrations of a flexible riser pipe by using multi-strip method

Muyu Duan[1,2], *Decheng Wan*[1] [*], *Hongxiang Xue*[1]

1. State Key Laboratory of Ocean Engineering, School of Naval Architecture, Ocean and Civil Engineering, Shanghai Jiao Tong University,
Collaborative Innovation Center for Advanced Ship and Deep-Sea Exploration, Shanghai, China
2. Department of Ship and Port Eng. ,Jiangsu Maritime Institue, Nanjing, Jiangsu, China
*Corresponding author

ABSTRACT

Vortex-induced vibration (VIV) is a key issue in deep water riser design. Design of deep water systems is a challenging engineering problem and the understanding of VIV and its suppression are very active areas of research. This paper presents the response of a vertical tension riser model in a step current when subject to VIV. The riser is 13.12m long and 28mm in diameter, with a mass ratio of 3.0. The simulation is carried out by a multi-strip method. This method combines a series of 2D RANS simulations of the flow at individual axial strips along the riser with a fully 3D FEM structural analysis based on Euler-Bernoulli beam theory. The entire flow-structure solution procedure is carried out in the time domain via a loose coupling strategy. The numerical results show that the VIV response is mainly dominated by the 7th mode for in-line vibrations and the 4th mode for cross-flow vibrations. The response included significant contributions from several modes. The riser pipe vibrates with a multi-modal pattern. Moreover, the dominant modes and modal amplitudes, the mean in-line displacement, and the instantons deflected shape of the riser in the cross-flow direction, etc., agree well with the experimental results. In particular, the numerically predicted location of the maximum mean in-line displacement and the experimental result differ by only about 1%. The good agreement between the numerical and experimental results shows that the multi-strip method is practical in predicting the general features as well as specifics of the VIV of the riser.

KEY WORDS: multi-mode response; vortex-induced vibration; vortex shedding; deep-water riser; lift and drag; long flexible cylinder

INTRODUCTION

Vortex-induced vibration (VIV) is a critical concern for the offshore industry for a variety of structures including pipelines, spar platforms, and risers. As oil exploration and production moves to increasingly deeper waters, there is a growing need to develop analytical methods for numerical analysis of long, flexible riser response. Vortex-induced vibration is a major cause of fatigue failure in offshore slender structures. The reliable estimation of fatigue damage of risers requires predictions of the presence and magnitude of VIV displacements and excitation modes in response to various current profiles and axial tensions, and is of practical interest to the industry.

Key features of offshore risers are that they have length-to-diameter of the order of at least 10^3, and that they undergo vibrations in high modes where the frequency intervals between adjacent modes are proportionally very small. Nevertheless, the ratio of the wavelength of any excited mode to the diameter of the riser is likely to be of order 10^2 . These features have restricted progress towards an understanding of the multi-mode response of risers to vortex excitation.

Over the past few decades, VIV of long flexible risers has been extensively studied. Many VIV experiments have been carried out for deepwater risers with high L/D, such as Chaplin et al (2005), Gu et al (2013), Tognarelli et al (2004), Tognarelli et al (2008), Trim et al (2005), Vandiver et al (2006). Chaplin et al (2005) carried out the experimental project in which a vertical model riser, 28 mm in diameter, 13.12 m long, was expected to a stepped current consisting of a uniform flow of up to 1 m/s over almost half of its length. The remainder of the riser was in the still water. Cross-flow vibrations were observed at modes up to the 8th, with standard deviations of individual modal weights greater than 50% of the riser's diameter. In-line vibrations were observed at modes up to the 14th.

Apart from the various experimental investigations, there have been several CFD studies on VIV of flexible cylinders with high L/D during the past few years. Whitney and Chung (1981) is one of the earliest researches of VIV of long pipes. Maximum RMS values of displacement and acceleration are presented for a range of speeds, pipe lengths, pipe diameters and wall thickness. Chung and Felippa (1981) gave the drag forces along the pipe and analyzed the three major factors affecting the forces. Willden and Graham (2001) used a quasi-three dimensional numerical method to simulate the VIV of a cylinder with L/D=100 that subject to a sheared inflow. Meneghini et al (2004) and Yamamoto et al. (2004) presented the numerical simulations of long marine risers with L/D up to 4600 using two-dimensional discrete vortex method (DVM). Menter et al (2006) first simulated riser VIV using fully three-dimensional (3D) finite volume method (FVM) and finite element method (FEM), respectively. Constantinides and Oakley (2008a; 2008b) presented the numerical simulations of long cylinders

with L/D=4200. Huang et al. (2009) performed finite-analytic Navier-Stokes (FANS) simulations of an L/D=482 cylinder. Nevertheless, three-dimensional fluid-structure interaction (FSI) simulations of VIV of vertical risers are still quite limited.

In this paper, a three-dimensional CFD approach is used to study the riser VIV responses in uniform currents and in-depth comparisons are made with experimental results. This approach is essentially a multi-strip numerical method, combing solutions of the incompressible Reynolds Averaged Navier-Stokes (RANS) equations with a finite-element structural dynamics analysis. More precisely, this solution methodology combines a series of 2D simulations of the flow at individual axial strips along the riser with a fully 3D structural analysis to predict overall VIV loads and displacements. An implementation of the flow-structure interaction technique into the open source code OpenFOAM is presented. The entire flow-structure solution procedure is carried out in the time domain via a loose coupling strategy, such that the hydrodynamic loads from each riser strip are summed to obtain the overall loading along the span of the riser.

In order to validate our approach, numerical simulations of the vortex-induced vibration of long-flexible risers were carried. The flow conditions and riser configuration are chosen according to experiments reported in Francisco (2006). The numerical results are compared with the benchmark data of Francisco (2006), and good agreement was achieved. The numerical results show that the VIV response is mainly dominated by the 7th mode for in-line vibrations and the 4th mode for cross-flow vibrations. The maximum in-line mean amplitude is $\overline{x}_{max}/D = 0.372$. The maximum cross-flow mean amplitude is $\overline{y}_{max}/D = 0.82$.

This paper is organized as follows: the first section gives a brief introduction to the numerical methods used to model the fluid and structural motion. The second section describes the problem and summarises the main parameter of the model riser. The natural frequencies and mode shapes of the riser are obtained in the next section. The fourth section presents overview of the computational domain. Grid convergence studies for the simulation of the flow around one strip of the riser are also carried out. The next section comprises two parts, namely in-line motion analysis and cross-flow motion analysis. In each part, time domain analysis, frequency domain analysis and mode analysis are conducted. The results compare well with the experimental data. The final section concludes the paper.

MATHMATICAL MODEL

Hydrodynamic Governing Equations

In this paper, the fluid is assumed to be incompressible and has constant density ρ and constant dynamic viscosity μ. The Reynolds-averaged Navier-Stokes equations are used as governing equations:

$$\frac{\partial \overline{u_i}}{\partial x_i} = 0 \tag{1}$$

$$\frac{\partial}{\partial t}(\rho \overline{u_i}) + \frac{\partial}{\partial x_j}(\rho \overline{u_i u_j}) = -\frac{\partial \overline{p}}{\partial x_i} + \frac{\partial}{\partial x_j}\left(2\mu \overline{S_{ij}} - \rho \overline{u_j' u_i'}\right) \tag{2}$$

where $\overline{S_{ij}} = \frac{1}{2}\left(\frac{\partial \overline{u_i}}{\partial x_j} + \frac{\partial \overline{u_j}}{\partial x_i}\right)$ is the mean rate of strain tensor. $-\rho \overline{u_j' u_i'}$ results from the fluctuating velocity field, and is generally referred to as the Reynolds stress τ_{ij}.

A turbulent model is required to compute the Reynolds stresses for turbulence closure. The SST $k-\omega$ turbulence model, which is

originally described by Menter (1994), is a two-equation eddy-viscosity model. Authors who use the SST $k-\omega$ model usually merit for its good behavior in adverse pressure gradients and separating flow. The Reynolds stress is modelled by a linear constitutive relationship using Boussinesq hypothesis with the mean flow straining field as

$$\tau_{ij} = -\rho \overline{u_j' u_i'} = 2\mu_t \overline{S_{ij}} - \frac{2}{3}\rho k \delta_{ij} \tag{3}$$

where μ_t is the turbulent viscosity, obtained from solving the SST $k-\omega$ model, $k = (1/2)\overline{u_i' u_i'}$ is the mean turbulent kinetic energy.

Applying Eq.3 to Eq.2, one has

$$\frac{\partial}{\partial t}(\rho \overline{u_i}) + \frac{\partial}{\partial x_j}(\rho \overline{u_i u_j}) = -\frac{\partial \overline{p_{eff}}}{\partial x_i} + \frac{\partial}{\partial x_j}\left(2\mu_{eff} \overline{S_{ij}}\right) \tag{4}$$

where $p_{eff} = p + \frac{2}{3}\rho k$, $\mu_{eff} = \mu + \mu_t$

The solution of the governing equations is achieved by using the PIMPLE (merged PISO-SIMPLE) algorithm, which is a large time-step transient solver for incompressible flow. PISO is an acronym for Pressure Implicit Splitting of Operators which is used for time dependent flows while SIMPLE for Semi-Implicit Method for Pressure Linked Equations which is used for steady state problems. In the SIMPLE algorithm, a pressure correction term is used while the velocity corrections are neglected because they are unknown. This results in rather slow convergence. The PISO algorithm also neglects the velocity correction in the first step, but them performs one in a later stage, which leads to additional corrections for the pressure. OpenFOAM utilizes collocated grids with all variables stored at cell centers and pressure and velocity coupled using the Rhie and Chow (1983) scheme.

Structural Dynamic Governing Equations

The structural dynamics solution procedure is based on a beam element representation using a consistent mass-matrix formulation. The resulting equations of motion for each structure are a set of second-order ODEs of the following form:

$$[M]\{\ddot{x}\} + [C]\{\dot{x}\} + [K - K_g]\{x\} = \{F_x\} \tag{5}$$

$$[M]\{\ddot{y}\} + [C]\{\dot{y}\} + [K - K_g]\{y\} = \{F_y\} \tag{6}$$

where x and y are the in-line and transverse displacements of the riser centroid at discrete locations along the span of the riser, $[M]$ is the mass matrix, $[C]$ is the damping matrix, $[K]$ is the stiffness matrix, and $[K_g]$ is the geometric matrix. The forcing functions, F_x and F_y, on the right-hand side of Eqs. (5) and (6) represent the hydrodynamic drag and lift forces acting on the structure. Note that the global mass, damping, and stiffness matrices are derived using small displacement Euler-Bernoulli beam theory comprised of 4 DOF elements (two transverse displacements and two angular displacements). Hence, each finite element contributes a 4×4 sub-matrix to the global matrices to obtain the overall structural dynamics formulation. Individual element contributions to the mass and stiffness matrix are presented as follows:

$$k_{ij} = \frac{2EI}{L^3}\begin{bmatrix} 6 & 3L & -6 & 3L \\ 3L & 2L^2 & -3L & L^2 \\ -6 & -3L & 6 & -3L \\ 3L & L^2 & -3L & 2L^2 \end{bmatrix} \tag{7}$$

$$m_{ij} = \frac{\overline{m}L}{420}\begin{bmatrix} 156 & 22L & 54 & -13L \\ 22L & 4L^2 & 13L & -3L^2 \\ 54 & 13L & 156 & -22L \\ -13L & -3L^2 & -22L & 4L^2 \end{bmatrix} \tag{8}$$

where EI is the bending stiffness, L is the length of the local finite

element, and $\bar{m}$ is the structural mass per unit length (Karl et al (2004)). The axial tension present in the riser is included through the addition of the geometric stiffness matrix, $[K_g]$, with individual element contributions defined as follows:

$$k_{gij} = \frac{-T}{30L}\begin{bmatrix} 36 & 3L & -36 & 3L \\ 3L & 4L^2 & -3L & -L^2 \\ -36 & -3L & 36 & -3L \\ 3L & -L^2 & -3L & 4L^2 \end{bmatrix} \qquad (9)$$

where T is the local axial tension force for each finite element. Note that the temporal integration of the structural dynamics equations of motion is carried out completely in the time domain using the Newmark beta method.

PROBLEM DESCRIPTIONS

The numerical simulation model of this paper follows Fransico et al (2006) experiments, the experimental device as shown in Fig.1. Note that the layout of this experiments is the same as the experiments of Chaplin et al (2005a).
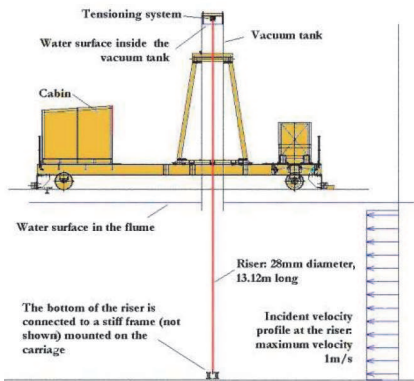
Fig. 1 Layout of the experiments of Fransico et al (2006)

The riser is 28mm in diameter and 13.12m long, with an aspect ratio of about L/D=469. The lower 45% of its length was subject to a uniform current, the rest was in still water. A top tension T is applied on the top end of the riser. The riser is pinned at both the top and bottom ends and free to move in the in-line (x) and cross-flow (y) directions. Detailed information about the riser is summarized in Table 1.

Table 1 Summary of main parameter of the model riser

External diameter	D	0.028	m
Length	L	13.12	m
Aspect ratio	L/D	469	-
Submerged Length	L_s	5.94	m
Flexural Stiffness	EI	29.88	Nm^2
Top Tension	T_t	1610	N
Flow speeds	V	0.605	m/s
Mass ratio	m^*	3	-
Mass ratio (bumpy cylinder)	m_b^*	3.1	-
Reynolds number	Re	16940	-

NATURAL FREQUENCIES AND MODE SHAPES

FEM calculated natural frequencies and mode shapes related to the first ten modes of the riser are presented. The natural frequencies and mode shapes are shown in Table 2 and Fig.2, respectively. Here, the top tension is taken as 1610 N. These results lay a foundation for the subsequent studies on multi-mode vortex-induced vibration of the riser.

Table 2 First ten natural frequencies - $T_t = 1610N$

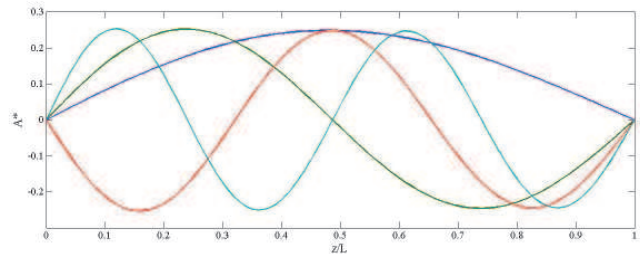| f_1 (Hz)	f_2 (Hz)	f_3 (Hz)	f_4 (Hz)	f_5 (Hz)
1.2237	2.4516	3.6878	4.9364	6.2014
f_6	f_7	f_8	f_9	f_{10}
7.4867	8.7961	10.133	11.520	12.906

Fig. 2 First four mode shapes - $T_t = 1610N$

COMPUTATIONAL DOMAIN

Geometry and Mesh Convergence Study

Twenty CFD strips are placed at equidistant locations along the portion of the riser below the water line, and ninety structural elements (ninety-one nodes) are used to discretize the beam. Fig.3 shows the distribution of strips along the span of the riser. Fig.4 illustrates the entire domain and the mesh of a strip. All grids used in this paper are structured grids, which ensure the quality of the grids and offer convenience to systematic refinement in all directions.
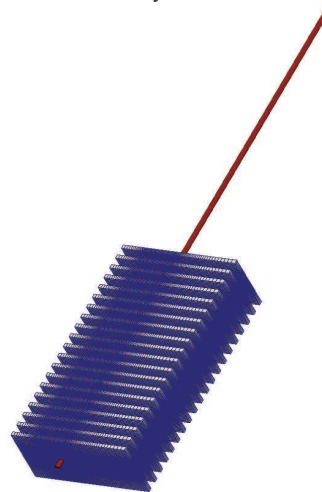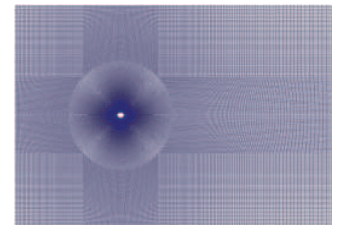

Fig. 3 illustration of multi-strip model

Fig. 4 geometry domain and entire mesh of a strip

Grid convergence studies for the simulation of the flow past one strip of the cylindrical riser are carried out. Here, the cylinder is kept

fixed. Simulations are performed with three different grid resolutions by varying the nodes around the cylinder and the distance of nearest grid to the cylinder boundary. Table 3 summarizes the information of the three meshes. In Table 3, the 'Quadrant' column lists the number of nodes for one quadrant of the cylinder, and the 'Radius' column shows the number of nodes in the radial direction between the cylinder and the outside concentric cycle.

Table 3 the details of three-meshes for the grid convergence study

Mesh	Number of Cells	Quadrant	Radius
Mesh I	46820	50	120
Mesh II	71653	75	180
Mesh III	98640	100	240

Table 4 presents comparisons between the average drag coefficients, rms lift coefficients and Strouhal number obtained in the present work for Reynolds number equals to 6.31×10^5, and experimental data from the literature. As shown in Table 4, the numerical results obtained in the present work for the three meshes agree well with the experimental data of ITTC C and Marin.

Table 4 Force coefficients and Strouhal numbers for different meshes and comparison with other results

Case	$C_{d.ave}$	$C_{l,rms}$	St
Mesh I	1.136	0.851	0.22
Mesh II	1.142	0.845	0.22
Mesh III	1.144	0.837	0.22
Marin (Exp.)	1.16	0.83	0.19
ITTC A	0.700	0.532	0.281
ITTC B	0.874	0.472	0.249
ITTC C	1.053	0.832	0.249

COMPUTATIONAL RESULTS AND DISCUSSION

Fig. 5 illustrates the vortex shedding along the riser at one moment. The alternate vortex shedding causes oscillatory drag and lift forces on the riser. These two forces then induce in-line and cross-flow riser motions, which in turn affect the vortex shedding. The in-line and cross flow motions are analyzed subsequently hereafter.Fig.6 is the time history of lift and drag coefficient at the tenth slice.
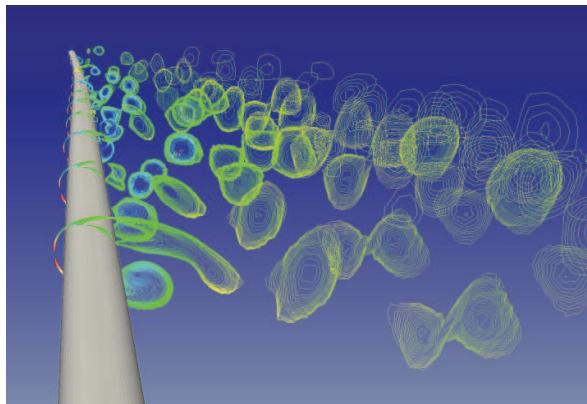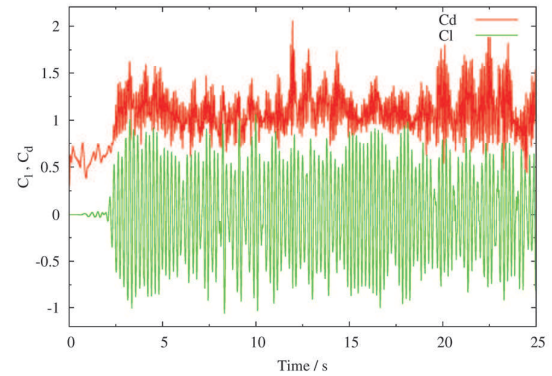

Fig. 5 vortex shedding along the riser at one moment

Fig.6 time history of lift and drag coefficient.

In-line Motion Analysis

Fig.7 depicts the time history of the in-line displacement at every ten equal segments along the span of the riser. As is shown in Fig.7, the displacement is relatively large in the middle part of the riser, and becomes smaller at both ends. The maximum displacement occurs not in the middle, but in the lower 30%-40% (the node number is 34 and the number of node is 1 to 91 from bottom to top) of the length. The in-line displacement of each node fluctuates around a mean position. Moreover, the fluctuation is more intense where the mean displacement is larger.
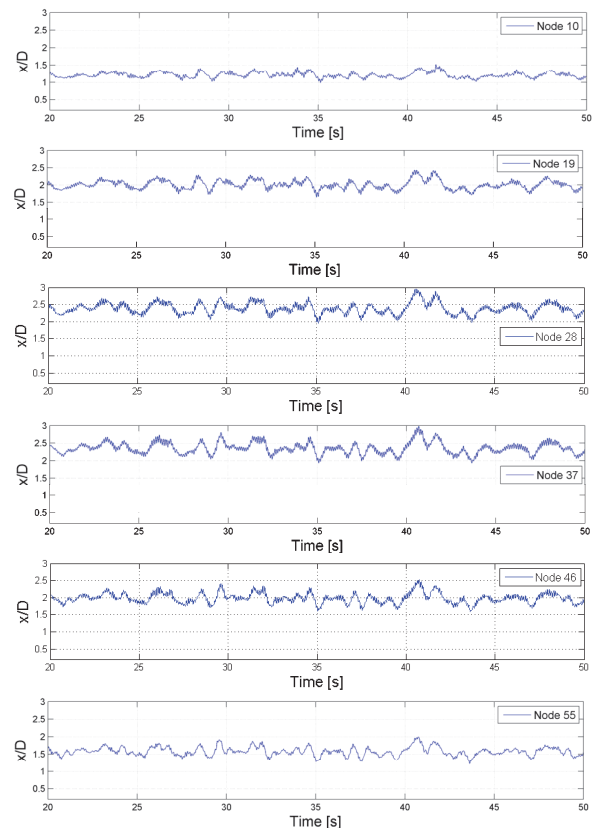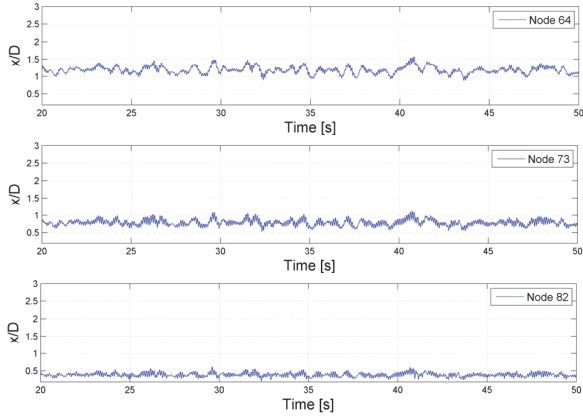
Fig. 7 Time history of the in-line displacement at the Node 10, 19, 28, 37, 46, 55, 64, 73, 82 (the node label is marked from the bottom to the top)

Fig.8 depicts the mean in-line displacement, plotted against the relative elevation z/L. The red line represents the experimental results and the blue line is the present numerical results. As already noted, the maximum displacement is not in the middle of the length because the displacement of the upper part of the riser (in still water) is smaller than the displacement of the lower part exposed to the current. The numerically obtained mean in-line displacement curve agrees well with the experimental one. Table 5 gives the value and location of the maximum in-line displacement. The numerical results is in good agreement with the experimental data. In particular, the present study predicts the location of the maximum displacement with the error of about 1.1%.

The root mean square value ($\tilde{s}$) of in-line displacement is defined as

$$\tilde{s} = \sqrt{\frac{1}{S}\sum_{i=1}^{S}\left[s_i(t)-\overline{s}\right]^2} \qquad (10)$$
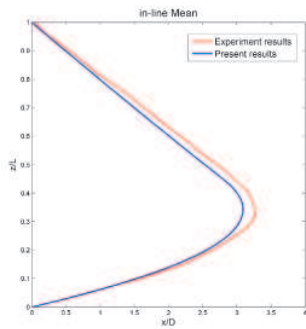
Fig. 8 The mean in-line displace−ment
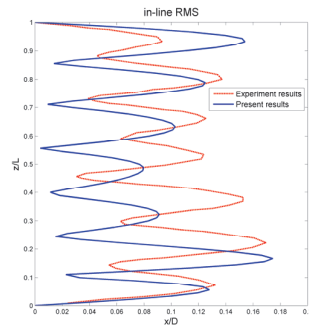
Fig. 9 The RMS of the in-line displacement

Table 5 the maximum of in-line mean displacement

	The maximum of in-line displacement ($\overline{x}/D$)	The location of maximum of in-line displacement (z/L)
Experiment	3.292	0.371
Present	3.072	0.367
Error / %	6.7	1.1

Fig.9 shows the RMS of the in-line displacement. The experimental

result is marked by a red curve and the present numerical result is marked by a blue curve. Fig.9 shows that the two RMS curves are consistent with each other. Both curves show that the RMS value of in-line vibration exhibits 7th mode shape. However, there are also other modes of vibration, otherwise the RMS node would be at $x/D=0$. Thus, the riser exhibits multi-mode vibration.

Fig.10 and Fig.11 shows the numerical and experimental results of the instantaneous spatio-temporal plot of the nondimensional in-line displacement from the mean position during three seconds. Fig.10 shows a very stable 7th mode. However, Fig.11 appears more complex. Fig.11 suggests that there are more than one type of mode shape during this period. Indeed, the dominant modes are the 7th and 8th mode, as shown further on. The mode transition between modes makes Fig.11 appears complicated.

The numerical results seems more practical because the Reynolds number is about 1.69×10^4. At this Reynolds number, the flow has transformed to purely turbulent. Although the wake vortex still shed from the riser at a certain frequency, the fluid flow is unstable. The turbulence has the characteristics of irregular, multi-scale and non-linear. Thus the fluctuating drag force imposed on the riser is inclined to cause multi-mode shape under this condition.
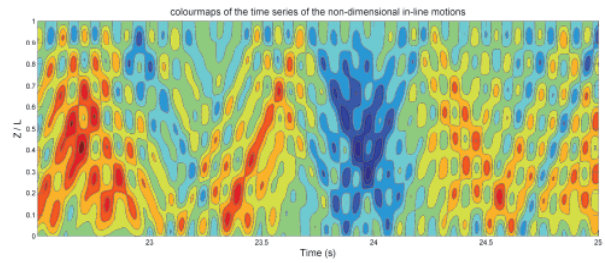

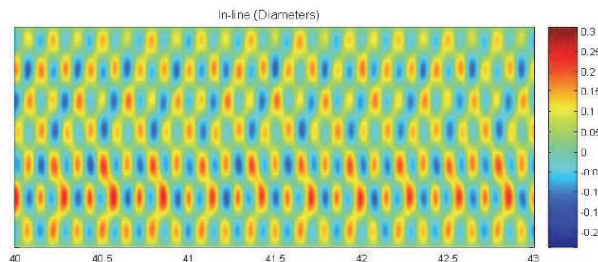Fig. 10 Spatio-temporal plot of non-dimensional in-line response

Fig. 11 Spatio-temporal plot of non-dimensional in-line response of experimental results of Francisco (2006)
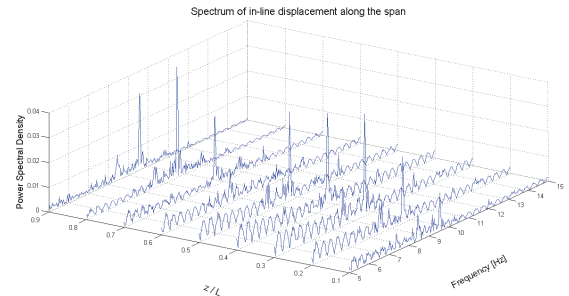

Fig. 12 The power spectra of the in-line displacement along the span

Fig.12 shows the power spectra of the in-line displacement of the node along the span. This figure is obtained via Fast Fourier Transformation (FFT) of the time history of the displacement. As shown in the Fig.12, the dominant frequencies where the largest spectral densities are found are almost the same and equal to 9.5526 Hz. The value of the dominant frequency is between the 7th and the 8th natural frequency, as demonstrated in Table 2.

Model analysis is now carried out. The time history of each displacement modal amplitude can be obtained as follows

$$A_x(t) = \Phi^{-1}(z)U(z,t) \tag{11}$$

where $\Phi = [\phi_1, \phi_2, \cdots, \phi_n]$ is the displacement modal shapes matrix and its column components are the non-dimensional displacement mode shapes normalized to be one at its maximum. $U(z,t)$ is the nodal displacements matrix, with the time series of the displacements being its row vectors, $U(z,t) = [u_1(t), u_2(t), \cdots, u_n(t)]$. $A_x(t)$ is the instantaneous displacement modal amplitudes matrix, and it has the same units as $U(z,t)$, because the mode shapes are non-dimensional.

Fig.13 depicts the first nine mode of displacement modal amplitudes in the case. Fig.14 shows the experimental results of Francisco (2006) under the same condition. As shown in Fig. , the response is mainly dominated by the 7th mode, consistent with the experimental data shown in Fig.11. However, Fig.13 also shows appreciable contribution from the 8th mode, which is consistent with the fact that the dominant frequency obtained via FFT of the displacement is between the 7th and the 8th natural frequency, as already noted. As shown in Fig.14, the envelope of the in-line displacement modal amplitude remains nearly constant at each mode, while Fig.13 shows that the envelopes of the amplitudes vary with time.
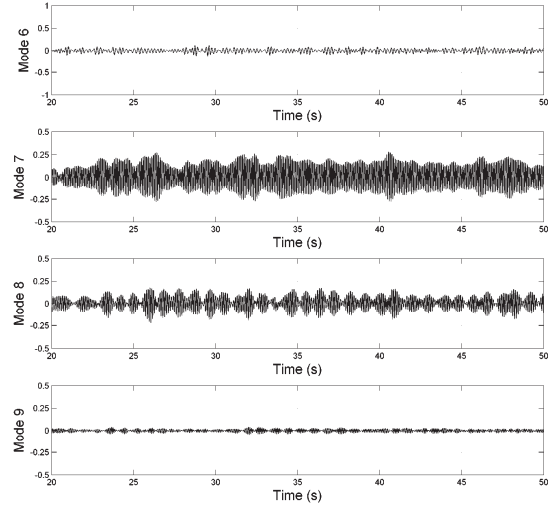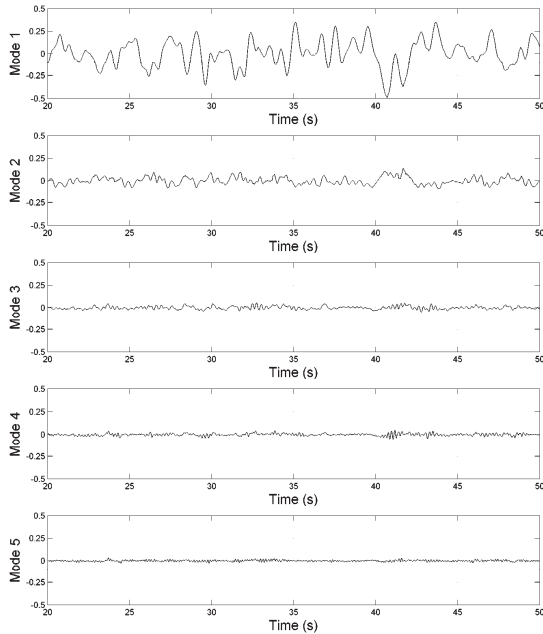

Fig. 13 Non-dimensional in-line displacement modal amplitudes from raw data- $T_t = 1610N, V = 0.605m/s$
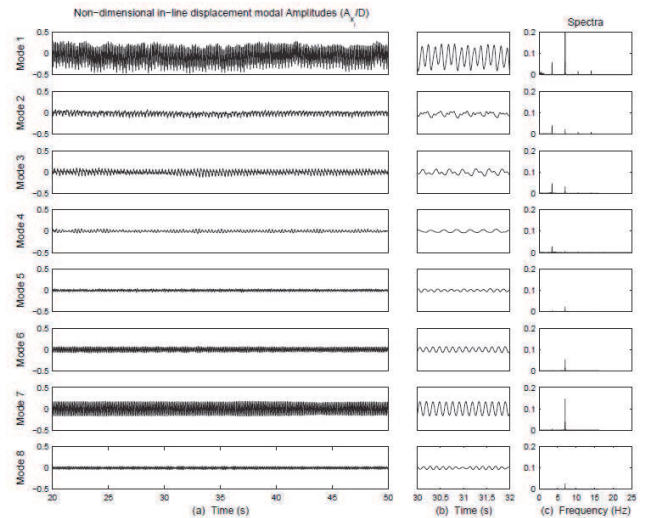

Fig. 14 Non-dimensional in-line displacement modal amplitudes from the experimental results of Francisco (2006)

Cross-flow Motion Analysis

The same procedure as in the previous section is applied to the analysis for the cross-flow motion of riser. First, the time history of the cross-flow amplitudes at every ten equal segments is given in Fig.15. The displacement of each node oscillates around $y/D = 0$. The amplitude of the oscillation changes over time.
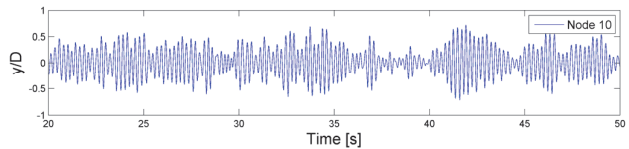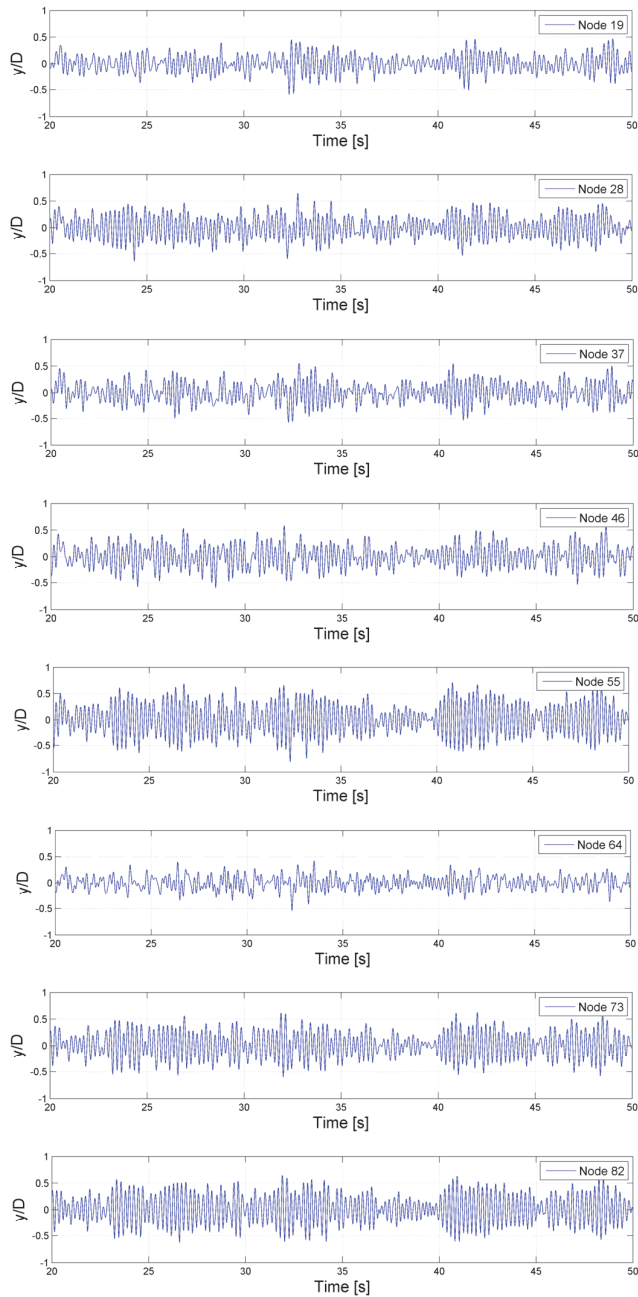
Fig. 15 Time history of the cross-flow displacements at the Node 10, 19, 28, 37, 46, 55, 64, 73, 82 (the node label is marked from the bottom to the top of the riser)
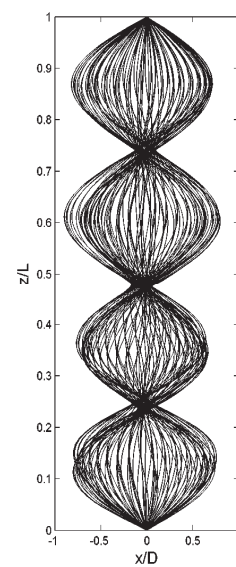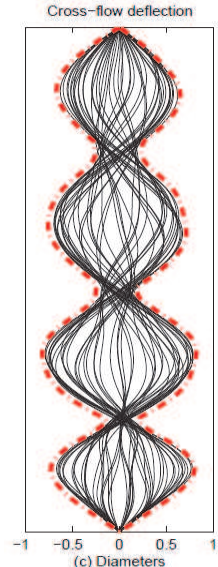

Fig. 16 Deflected shapes of the riser

Fig. 17 Deflected shapes of the riser obtained by experiment

Typical instantaneous deflected shapes of the riser and the relevant experimental results are shown in Fig.16 and Fig.17, where cross-flow displacements are plotted against the relative elevation z/L. Continuous lines in Fig.16 plot the positions of the riser at intervals of 0.01s through a time period (1 second) of the cross-flow oscillation. The numerical results agree well with the experimental data not only in the mode shape but also in the predicted amplitude. A typical feature of the results, demonstrated in the figures, is that displacements of the upper part of the riser (in still water) are no smaller than those exposed to the current below. The maximum cross-flow amplitude is $\bar{y}_{max}/D = 0.82$.

Fig.18 shows the spatio-temporal plot of non-dimensional cross-flow response, obtained by numerical simulation. Fig.18 shows that the dominant mode shape is controlled by the 4th mode, which agrees well with the experimental data of Francisco (2006), as shown in Fig.19. Compared with the in-line vibration mode, the cross-flow vibration mode is much more stable.
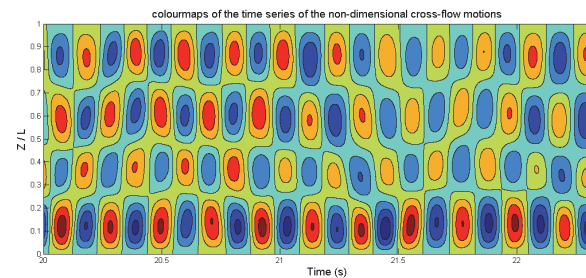

Fig. 18 Spatio-temporal plot of non-dimensional cross-flow response
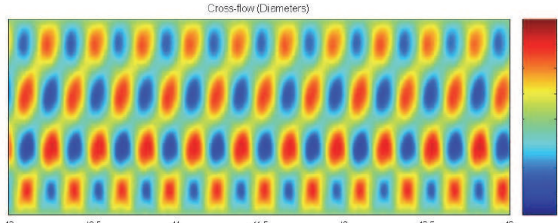
Fig. 19 Spatio-temporal plot of non-dimensional cross-flow response of experimental results of Francisco (2006)

Fig.20 depicts the power spectra of the cross-flow displacements at nine equally spaced nodes along the span of the riser, obtained via FFT of cross-flow displacement data. Fig.20 shows that the dominant frequencies of vibration at each node are the same and equal to 4.4558 Hz. This value is very close to the 4th natural frequency, as shown in Table 2. The dominant frequency of in-line direction is about twice that of the cross-flow direction.
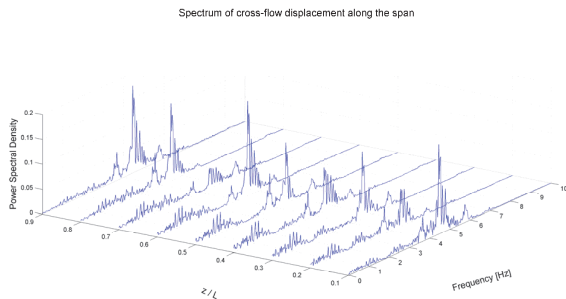

Fig. 20 The power spectra of the cross-flow displacements along the span

We continue to carry out the mode analysis of cross-flow vibration. Fig.21 depicts the first nine non-dimensional cross-flow displacement modal amplitudes. As shown in Fig.21, the response is mainly dominated by the 4th mode, which agrees well with the experimental data, as shown in Fig.22. The modal amplitudes of the 6th, 7th, 8th and 9th mode is very small and can be ignored. And there is evidence of simultaneous contributions from modes on either side of the dominant mode. The situation of cross-flow mode is very similar to the in-line mode, where the envelope of the modal amplitude of each mode is not a constant but varies with time.
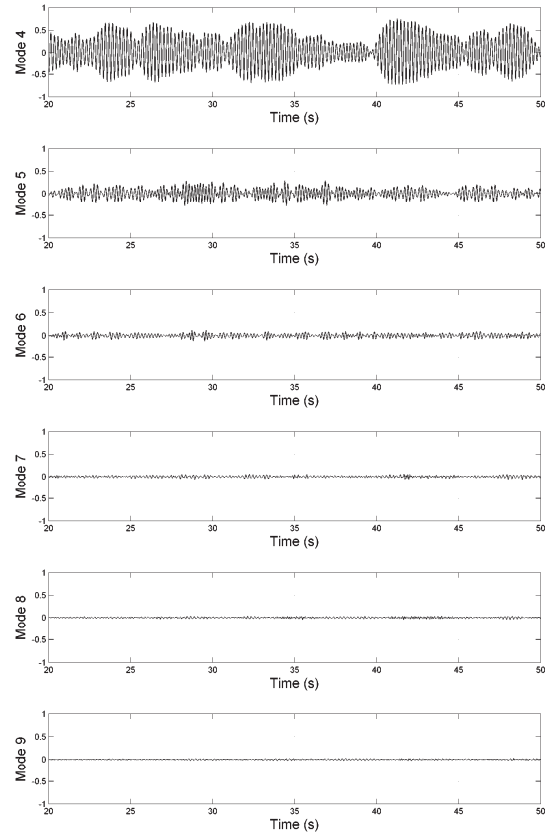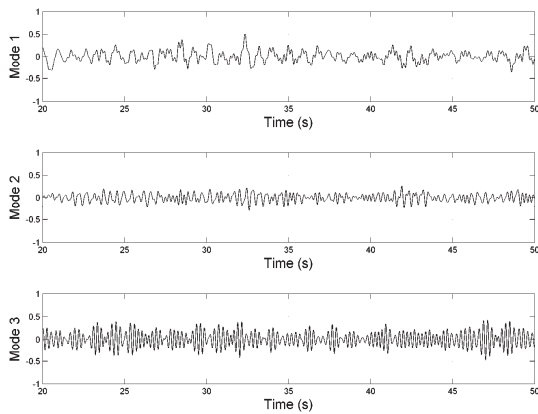

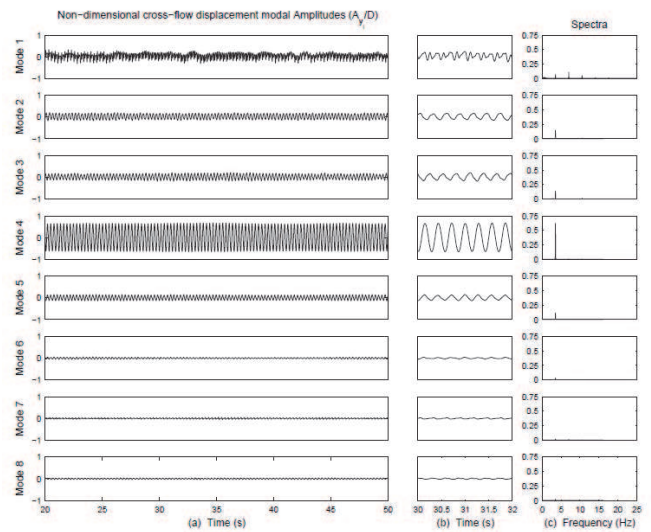Fig. 21 Non-dimensional cross-flow displacement modal amplitudes

Fig. 22 Non-dimensional cross-flow displacement modal amplitudes from the experimental results of Francisco (2006)

1072

CONCLUSIONS

In this study, we carried out numerical simulations of vortex-induced vibrations of a vertical tension riser in a stepped current. A multi-strip method numerical method has been developed combining a number of two dimensional RANS solutions with a three-dimensional finite element method based on Euler-Bernoulli beam theory. The good agreement between the numerical and experimental results show that the multi-strip method is reliable. The vibration response is analyzed in detail in in-line and cross-flow direction respectively. Lots of conclusions are drawn and a remarkable insight into the physics of vortex-induced vibration of long flexible riser is gained.

The numerical results show that the numerically predicted mean in-line displacement and the experimental result have great consistency. The structural nodes all respond at the same frequency. The frequency of in-line direction is 9.5526 Hz, which is between the 7th and the 8th natural frequency. And the frequency of cross-flow direction is 4.4558 Hz, which is very close to the 4th natural frequency. The results of mode analysis are very consistent with the frequency results. The riser vibrates in the 7th and the 4th modes in the in-line and cross-flow directions, respectively. But the situation of the riser vibration is not stable. Mode transition among different modes is happened occasionally, especially for the modes on either side of the dominant mode. The long flexible riser pipe vibrates in multi-mode pattern. The multi-mode vibration of the riser might be due to the fluctuating drag and lift forces imposed on the riser because of the turbulent flow. The overall good agreement between numerical results and experimental data show that the multi-strip method is practical in predicting the characteristics of the VIV response of the riser both qualitatively and quantitatively.

REFERENCES

Chaplin, J.R., Bearman, P.W., Huera Huarte, F.J., Pattenden, R.J., 2005. Laboratory measurement of vortex-induced vibrations of a vertical tension riser in a stepped current. J. Fluids Struct. 21,3-24.

Chung, J.S., Felippa, C.A., 1981. Nonlinear static analysis of deep ocean mining pipe – Part II: numerical studies. J. Energy Resour. 103,16-25.

Constantinides, H., Oakley, O.H., 2008a. Assessment of empirical VIV analysis tools and benchmark with experiments, OMAE2008-57216, Proc. 27th OMAE Conf., Estoril, Portugal.

Constantinides, H., Oakley, O.H., 2008b. Numerical prediction of VIV and comparison with field experiments, OMAE2008-57215, Proc.27th OMAE Conf., Estoril, Portugal.

Francisco, J.H.H., 2006. Multi-mode vortex-induced vibrations of a flexible circular. phD thesis, the University of London.

Gu, J., Vitola, M., Coelho, J. Pinto, W., Duan, M., Levi, C., 2013. An experimental investigation by towing tank on VIV of a long flexible cylinder for deepwater riser application. J. Mar. Sci. Technol. 18, 358-369.

Huang, K., Chen, H.C., Chen, C.R., 2009. Vertical riser VIV simulation in uniform current. J. Offshore Mech. Arct. Eng. 132,1-10.

Meneghini, J.R., Saltara, F., Fregonesi, R.A., Yamamoto, C.T., Casaprima, E., Ferrari, J.A., 2004. Numerical simulation of VIV on long flexible cylinders immersed in complex flow fields. Eur. J. Mech. B/Fluids 23, 51-63.

Menter, F., Sharkey, P., Yakubov, S., Kuntz, M., 2006. Overview of fluid-structure coupling in ANSYS-CFX, OMAE2006-92145, Proc. 25th OMAE Conf., Hamburg, Germany.

Tognarelli, M.A., Slocum, S.T., Frank, W.R., Campbell, R.B., 2004. VIV response of a long flexible cylinder in uniform and linearly sheared currents, OYC 16338, Proc. 2004 Offshore Tech. Conf., Houston, Texas, USA.

Tognarelli, M.A., Taggart, S., Campbell, M., 2008. Actual VIV fatigue response of full scale drilling riser: with and without suppression devices, OMAE2008-57046, Proc. 27th OMAE Conf., Estoril, Portugal.

Trim, A.D., Braaten, H., Lie, H., Tognarelli, M.A., 2005. Experimental investigation of vortex-induced vibration of long marine risers. J. Fluids Struct. 21, 335-361.

Vandiver, J.K., Swithenbank, S., Jaiswal, V., Marcollo, H., 2006. The effectiveness of helical strakes in the suppression of high-mode-number VIV, OTC 18276, Proc. 2006 Offshore Tech.,Conf., Houston, Texas, USA.

Whitney A.K., Chung J.S., 1981. Vibrations of long marine pipes due to vortex shedding. Journal of Energy Resources Technology. 103,231-236.

Willden, R.H.J., Graham, J.M.R., 2001. Numerical prediction of VIV on long flexible circular cylinders. J. Fluids Struct. 15, 659-669.

Yamamoto, C.T., Meneghini, J.R., Saltara, F., Fregonesi, R.A., Ferrari, J.A., 2004. Numerical simulations of vortex-induced vibration on flexible cylinders. J. Fluids Struct. 19, 467-489.